Journal of Materials Chemistry B

PAPER

View Article Online
View Journal | View Issue

Cite this: J. Mater. Chem. B, 2015, 3, 1507

Reversible PEGylation and Schiff-base linked imidazole modification of polylysine for high-performance gene delivery

Xiaojun Cai,[ab] Yongyong Li,*[b] Dong Yue,[a] Qiangying Yi,[a] Shuo Li,*[ac] Donglu Shi[b] and Zhongwu Gu*[a]

Received 17th October 2014
Accepted 2nd November 2014

DOI: 10.1039/c4tb01724b

www.rsc.org/MaterialsB

Gene carriers made from polylysine are of interest in relation to gene therapy but suffer from the lack of transfection efficiency due to limited stability and endosomal escape ability. To address this problem, we designed and developed Schiff-base linked imidazole modified polylysine with a reversible-PEGylation cationer (SL-ImPEG-SS-PLL) for high efficiency gene delivery. The reversible PEGylation was introduced for *in vivo* circulation, as well as selective PEG detachment to augment the cellular internalization, while introducing Schiff-base linked imidazole residues into polylysine was expected to accelerate the endosomal escape of the DNA payload, as well as facilitate intracellular DNA unpacking and release, thus significantly enhancing gene delivery efficiency. The size alteration of the SL-I_{15}mPEG-SS-PLL/pDNA polyplexes in the presence of 10 mM GSH suggests stimulus-induced PEG detachment under tumor relevant reduction conditions. Acid–base titration assays indicate that imidazole residues confer on polylysine remarkable buffering ability. The agarose gel retardation assay suggests that the Schiff-base linkages provide an increased DNA binding ability to protect DNA against nucleases and timely intracellular DNA unpacking to permit DNA dissociation from polylysine and access to transcriptional machinery. Biological efficacy assessment of this multifunctional carrier, using pEGFP and pGL-3 as reporter genes, indicates comparable to or even higher transfection efficiencies than gold standard PEI and their transfection efficiencies are slightly affected by serum. More importantly, *in vivo* transfection of pEGFP reveals that GFP expression was found not only in some of the important organs, such as the liver, spleen, kidneys and lungs, but also in the transplanted carcinoma. These experimental results suggest that the reversible PEGylation and Schiff-base linked imidazole modification make SL-ImPEG-SS-PLL a great potential candidate for an effective and biocompatible gene delivery system.

Introduction

Gene therapy is considered to be one of the most promising approaches to treat diseases of genetic defects.[1–3] Successful gene therapies, however, strongly depend on the development of effective and safe gene delivery vectors that are capable of mediating high and sustained levels of gene expression.[4–8] While viral vectors, such as adenoviruses and retroviruses can mediate highly efficient gene transfer, they pose safety issues such as healthy cell inflection, inflammation, immunogenicity, carcinogenicity, and the possibility of gene recombination, which prompted parallel pursuit for non-viral vectors.[9–12]

Synthetic cationic polymers as one of the main classes of non-viral vectors offer new opportunities for relatively safe gene delivery because they regularly induce a low immune response and have advantages such as high gene-loading capacity, handy chemical modification, and large-scale production.[13–16] Various cationic polymers such as polyethylenimine (PEI),[17,18] polylysine (PLL),[19,20] polyamidoamine (PAMAM),[21–23] poly(2-dimethylaminoethyl methacrylate) (pDMAEMA)[24,25] and poly(β-amino esters) (PBAEs)[26] have been extensively investigated as versatile gene carriers. These vectors can condense nucleic acids to nano-sized complexes (polyplexes), which can protect nucleic acids from extracellular enzymatic degradation, and enter cells *via* endocytosis followed by releasing the genes inside the cytoplasm or nucleus of the cells.[27] However, gene therapy based on these vectors still remains a great challenge due to the multiple hurdles during the delivery processes such as low colloidal stability during circulation, inefficient endocytosis, slow endosomal escape, untimely or incomplete DNA unpacking and

[a]National Engineering Research Center for Biomaterials, Sichuan University, Chengdu 610064, China. E-mail: zwgu@scu.eud.cn; Fax: +86 28 85410653; Tel: +86 28 85412923

[b]The Institute for Biomedical Engineering and Nano Science, Tongji University School of Medicine, Tongji University, Shanghai, 200120, China. E-mail: yongyong_li@tongji.edu.cn; Fax: +86 21 65983706; Tel: +86 21 65983706

[c]School of Chemical Engineering, Chongqing University of Technology, Chongqing 400054, China

release and poor nuclear import.[28–30] Although methodologies exist or are under development for solving individual barriers in the polymeric gene delivery processes, it is eventually a big challenge to design a multifunctional polymeric system with multiple features incorporated and optimized to overcome these hurdles collectively to achieve a highly efficient and safe gene delivery.[27,31–33]

Polylysine (PLL) is a conventional cationic polymer well known for its appreciable gene loading capacity and biodegradability. However, its lack of stability and capability of endosomal escape has posed some limitations in the biomedical applications.[34–36] Recently, we have developed a reversible PEGylated polylysine that can efficiently pack genes and remain intact extracellularly while triggering PEG detachment according to the intracellular glutathione (GSH) level.[29,37] The key structural factor of this system relies on the disulfide link between the two blocks of PEG and polylysine. The redox-responsive properties of the disulfide bond allow the selective detachment of PEG, facilitating the cellular internalization and intracellular release/transfer of the payload gene. The unique polylysine vector has been found to enhance the serum stability and gene transfection efficiency. However, the biological efficiency of this vector still cannot meet the requirements for clinical gene therapy, which can be ascribed to its inherent limited endosomal escape ability. Besides, inefficient intracellular DNA unpacking and release may also be regarded as one important rate-limiting step for PLL, because cationic polymers with positive charges condense DNA so tightly that it becomes increasingly difficult for the packed gene to dissociate from its carriers, seriously limiting the ultimate gene transfection.[4] Hence, a masterly structural design and optimization are crucial for developing a promising PLL system with an optimal balance between DNA protection and release, as well as efficient endosomal escape.

An imidazole ring is a functional moiety of many biomolecules (such as histidine) and has frequently been incorporated into polymeric vectors to increase their biocompatibility and gene transfection efficiency because the imidazole heterocycle possesses large proton buffering capacity at the endosomal/lysosomal pH range.[30,38,39] For example, imidazole-chitosan prepared through the EDC (1-ethyl-3-(3-dimethylaminopropyl) carbodiimide) chemistry has been successfully developed and used for nucleic acid delivery.[40,41] However, the amide linkage between the imidazole ring and chitosan might be easily digested by enzymes *in vivo*.[42] In contrast to amide bonds, Schiff-base linkages are more preferred to develop an intracellular microenvironment responsive polymeric gene delivery system because of their specific molecular properties. The pK_a of a Schiff-base (–N=C*H*–) is between 10.6 and 16.0 at 25 °C, and it can be fully protonated at physiological pH,[43] which results in the improvement of gene-binding ability.[44] In addition, the Schiff-base is endosomal pH sensitive and it can remain intact at physiological pH during hydrolysis in a weakly acidic endosomal microenvironment (5.0–6.5),[45,46] which will conversely reduce the gene loading capacity and facilitate intracellular DNA unpacking and release.[3] Based on these findings, we hypothesize that the Schiff-base linked imidazole residues may serve as promising multifunctional moieties for the development of a highly efficient and biocompatible polymeric gene delivery system with efficient endosomal escape ability as well as good balance between DNA protection and release.

As a proof of concept, we engineered and developed a unique Schiff-base linked imidazole modified polylysine with a reversible-PEGylation catiomer (SL-ImPEG-SS-PLL) for high efficiency gene delivery. The endosomal escape capability, as well as DNA protection and release behaviour was evaluated using acid–base titration measurements, agarose gel electrophoresis and dynamic laser light scattering. The reversible PEGylation was investigated by DLS. The physicochemical properties (particle size, zeta potential and morphology), bio-safety, transfection efficiency *in vitro* and *in vivo* were also investigated.

Results and discussion

Synthesis and characterization of Schiff-base linked imidazole modified polylysine with a reversible-PEGylation catiomer (SL-ImPEG-SS-PLL)

The Schiff-base linked imidazole modified polylysine with a reversible PEGylation catiomer (SL-ImPEG-SS-PLL) was designed with a redox-sensitive disulfide bond between the PEG and PLL moieties in addition to Schiff-base linkers between lysine units and imidazole. The design rationale is based on the desire to detach the external PEG shell in the presence of tumor-relevant GSH concentrations for facilitating intracellular uptake of PLL/DNA complexes. Following successful internalization into target cells, the protonation of imidazole groups will lead to the influx of chloride ions, osmotic swelling and rupture of endosomes, which can accelerate the escape of DNA complexes from late endosomes to the cytoplasm. In the meantime, the hydrolysis of Schiff-base linkers in a weakly acidic endosomal microenvironment will facilitate the intracellular DNA unpacking and release, which is a necessary prerequisite for gene transfer into the nucleus.

The synthesis of this multifunctional catiomer is illustrated in Fig. 1. In brief, mPEG-SS-PzLL$_{52}$ was prepared by the ring-opening polymerization of zLL-NCA using mPEG-SS-NH$_2$ as an initiator. After deprotection, the imidazole rings were introduced into the side chains of PLL *via* the reaction of the amino group of mPEG-SS-PLL$_{52}$ and the aldehyde group of 4-imidazolecarboxaldehyde at RT, where Schiff-base linkers were formed. The number of imidazole residues on one mPEG-SS-PLL$_{52}$ molecule was optimized by varying the feed ratio of 4-imidazolecarboxaldehyde to mPEG-SS-PLL$_{52}$, from 1 : 10 to 1 : 4. The successful synthesis of mPEG-SS-PLL$_{52}$ and SL-ImPEG-SS-PLL with different imidazolyl substitutions was demonstrated by ^{1}H NMR spectra as shown in Fig. 2. In addition to distinct resonance peaks for the PEG and PLL blocks, the presence of proton signals at δ 9.6 ppm indicates the formation of Schiff-base (–*H*C=N–) linkages. Moreover, the successful synthesis of SL-ImPEG-SS-PLL can be further confirmed by the presence of imidazole rings with their proton chemical shifts at $\delta \approx$ 7.2–7.5 ppm. The average number of imidazole residues bound per mPEG-SS-PLL$_{52}$ molecule was calculated to be 3, 6

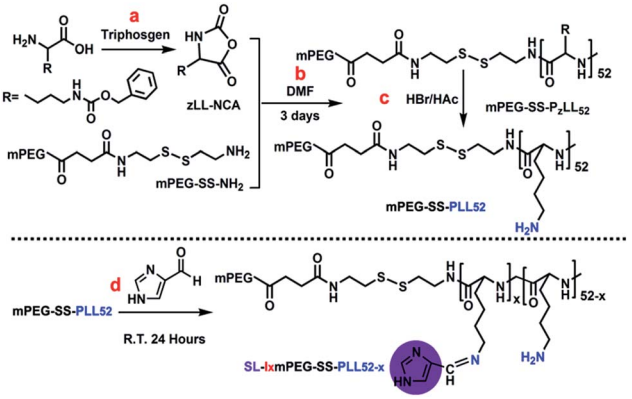

Fig. 1 Synthetic scheme of SL-ImPEG-SS-PLL, (a) zLL/triphosgene = 2.4 : 1, mol/mol, THF, 50 °C, 4 h; (b) zLL-NCA/mPEG-SS-NH_2 = 60 : 1, mol/mol, DMF, RT, 3 days; (c) mPEG-SS-PzLL$_{52}$, TFA, HBr/HAc, 0 °C, 1 h; (d) mPEG-SS-PLL$_{52}$ is substituted with 4-imidazolecarboxaldehyde.

and 15, respectively, by comparing the integration values of proton peaks of Schiff-base linkages (9.6 ppm) and proton peaks of lysine (0.97–1.79 ppm). Hence, the final products are designated as SL-I_3mPEG-SS-PLL, SL-I_6mPEG-SS-PLL and SL-I_{15}mPEG-SS-PLL, respectively.

Cellular viability assessment

The clinical success of synthetic gene delivery vectors critically depends on meeting an acceptable safety profile in addition to therapeutic efficacy. As a promising alternative for viral vectors, catiomers exhibit good prospects, while having potential toxicity because of their membrane-disruptive ability.[28] Hence, cell viability assessment was performed here to assess the biosafety of fabricated catiomers using the 293T and MCF-7 cell lines. As shown in Fig. 3, cell viability rapidly decreased to a limiting value around 30% at concentrations >30 mg L^{-1}, in the presence of bPEI-25k (positive control). Previous studies demonstrated that the cationic charge density of PEI is responsible for this dramatic reduction in cell viability.[47] In contrast, mPEG-SS-PLL$_{52}$-based polymers exhibited a

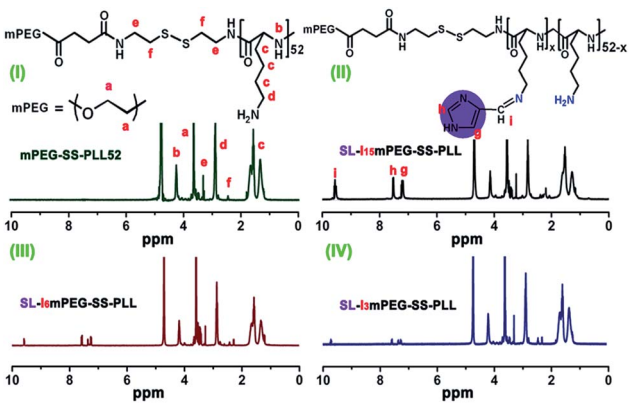

Fig. 2 ^{1}H NMR spectra of fabricated catiomers, (I) mPEG-SS-PLL$_{52}$, (II) SL-I_{15}mPEG-SS-PLL, (III) SL-I_6mPEG-SS-PLL and (IV) SL-I_3mPEG-SS-PLL in D_2O.

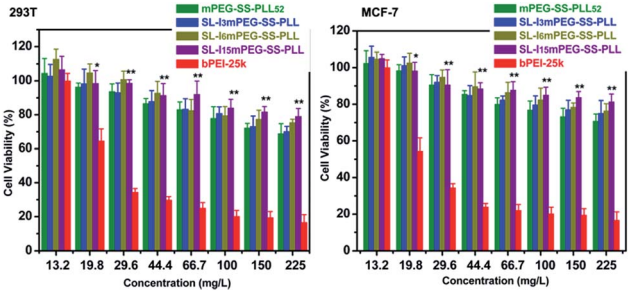

Fig. 3 Dose-dependent cytotoxicity of SL-ImPEG-SS-PLL-based catiomers. The viability of 293T (A), and MCF-7 (B) cells following a 24 h incubation with various concentrations of PEI (positive control), or SL-ImPEG-SS-PLL-based catiomers was quantified using the MTT assay. Data are shown as mean ± SD (n = 5) (*p < 0.05, **p < 0.01, SL_{15}-ImPEG-SS-PLL *vs.* bPEI-25k).

remarkably increased cellular viability profile even at concentrations of 225 mg L^{-1}. Throughout the entire concentration range tested, the cell viability was always maintained >70% following a 24 h incubation. These results are in good agreement with our previous reports that limited interaction and can reduce cytotoxicity owing to the PEG-shielding effect.[37] Besides, it is worth noting that SL-ImPEG-SS-PLL exhibits slightly higher cell viability in comparison to mPEG-SS-PLL$_{52}$. The possible reason may be ascribed to the reduction in the number of toxic primary amino groups as well as the presence of imidazole residues, as it is reported that a protonated imidazole ring is less cytotoxic than protonated amines.[48]

DNA binding ability and buffering capacity of the SL-ImPEG-SS-PLL catiomer

Electrostatic interactions between negatively charged DNA and positively charged polymers facilitate the formation of partially or completely neutralized association polyplexes. As a consequence, the successful condensation of DNA with catiomers results in the retardation or complete loss of oriented migration of DNA within an electric field. As evident from Fig. 4A, DNA migration is efficiently inhibited by the mPEG-SS-PLL$_{52}$/pDNA complexes at a weight ratio >0.5, indicating effective DNA condensation. Introducing Schiff-base linked imidazole residues into the side chains of polylysine further increased the

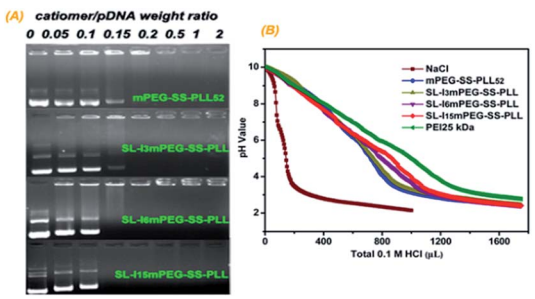

Fig. 4 Gel retardation assay of various catiomers complexed with plasmid DNA (A). Buffering capacities of bPEI-25k, mPEG-SS-PLL$_{52}$, SL-I_3mPEG-SS-PLL, SL-I_6mPEG-SS-PLL and SL-I_{15}mPEG-SS-PLL (B).

gene loading capability of mPEG-SS-PLL$_{52}$ because the Schiff-base linkage (pK_a: 10.6–16.0) provides a stronger binding affinity with pDNA than the amino group of polylysine (pK_a: 9.0), which is consistent with the previous report that polymers with a higher pK_a value can form stable polyplexes even at lower N/P ratios.[49] As a consequence, SL-I$_3$mPEG-SS-PLL, SL-I$_6$mPEG-SS-PLL and SL-I$_{15}$mPEG-SS-PLL reach complete retardation of pDNA at a weight ratio of 0.2, 0.2 and 0.15, respectively.

Optimal gene transfection requires transfer of the genetic payload into the nucleus. Following cellular internalization, escape from endosomal vesicles represents a major limitation for gene delivery systems. The proton sponge effect has been reported to be a key factor in the swelling of the endocytic vesicles, escaping into the cytosol, and therefore affecting the overall gene transfection efficiency. Our previous studies have shown the limited buffering capacity of mPEG-SS-PLL, primarily due to the lack of secondary and tertiary amines,[37] which greatly impedes the transgene expression. To overcome this critical barrier, imidazole residues were chemically conjugated to the side chains of polylysine *via* the Schiff-base reaction. The buffering capacity of mPEG-SS-PLL$_{52}$ and SL-ImPEG-SS-PLL was evaluated using the conventional acid–base titration method. The results from these titration experiments are summarized in Fig. 4B. Consistent with previous findings, mPEG-SS-PLL$_{52}$ exhibits a limited buffering capacity attributable to its uniform composition of primary amines.[37] However, with the incorporation of imidazole residues, a remarkable increase in the buffering capacity of the SL-ImPEG-SS-PLL catiomer is observed, possibly associated with the intrinsic proton sponge effect of the imidazole heterocycle at the endosomal/lysosomal pH range. In addition, the buffering capacity of SL-ImPEG-SS-PLL catiomers shows a slight increase with increasing imidazolyl substitution. These results indicate that imidazole modification can efficiently increase the buffering capacity of mPEG-SS-PLL$_{52}$, which has an important function in facilitating genetic payload release into the cytoplasm.

Complexes of pDNA with SL-ImPEG-SS-PLL catiomers

The particle size and surface charge of catiomer/pDNA polyplexes are known to strongly influence the cytotoxicity, cellular uptake, intracellular trafficking, release of genetic payload, and subsequent transfection efficiency.[50,51] The morphometric analysis of SL-ImPEG-SS-PLL/pDNA complexes was performed by transmission electron microscopy (TEM) and dynamic light scattering (DLS). The particle size distribution shown in Fig. 5A reveals the near-Gaussian distribution of SL-I$_{15}$mPEG-SS-PLL/pDNA polyplexes between 100 and 300 nm, with a mean diameter of ~180 nm. The inset in Fig. 5A shows a representative TEM image where SL-I$_{15}$mPEG-SS-PLL/pDNA polyplexes are visible as spherical aggregates with diameters between 40 and 60 nm. The apparent discrepancy in size characteristics between the two methods is predicted to arise from the evaporation of water required during TEM sample preparation. Similar results were also observed in Fig. 5B, in which mPEG-SS-PLL$_{52}$/pDNA polyplexes have a mean dynamic hydration

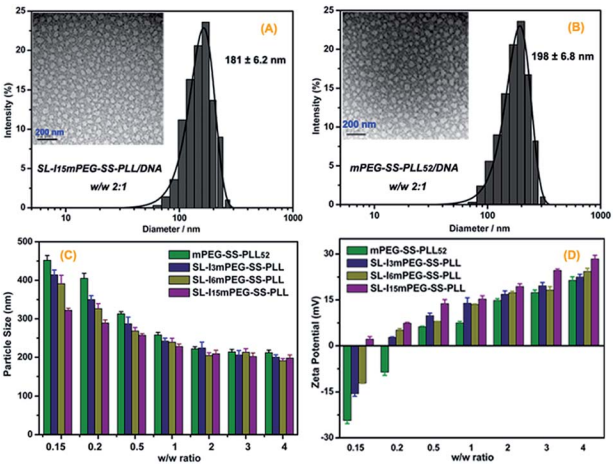

Fig. 5 Typical TEM images (inset) and size distribution of the (A) SL-I$_{15}$mPEG-SS-PLL/pDNA and (B) mPEG-SS-PLL$_{52}$/pDNA polyplex; (C) mean particle size and (D) zeta potential of the mPEG-SS-PLL$_{52}$/pDNA and SL-I$_{15}$mPEG-SS-PLL/pDNA polyplex, fabricated in 150 mM NaCl at various weight ratios. Data are shown as mean ± SD (n = 3).

diameter around 200 nm, while being present as spherical aggregates with diameters between 50 and 60 nm under TEM observation.

The impact of different polymer/pDNA weight ratios on the mean particle size and zeta potential of polyplexes is summarized in Fig. 5C and D. These data show a similar tendency that the particle size decreases with increasing weight ratios, and the average particle size is less than 210 nm at weight ratios ≥2 : 1, which is considered to be the suitable size range for efficient cellular uptake and circulation.[52] In parallel, the zeta potential of these complexes significantly increases from −24 to +28 mV when the catiomer/pDNA weight ratio is increased from 0.15 : 1 to 4 : 1. The dramatic shift in zeta potential indicates the gradual neutralization of the negative charge of polymer-associated pDNA. The neutralization appears at a weight ratio of 0.2 : 1. These results are consistent with previous electrophoretic mobility data shown in Fig. 4A. Further increase in the catiomer content leads to an excess of positively charged amine groups on the surfaces of the polyplexes. Eventually, charge–charge repulsion limits particle formation to a mean diameter less than 210 nm and zeta potential of +28 mV. It should be noted that throughout the entire weight ratio range tested, the SL-ImPEG-SS-PLL/pDNA polyplexes always maintained a smaller particle size and higher zeta potential compared to those of mPEG-SS-PLL$_{52}$/pDNA polyplexes, primarily owing to its stronger DNA binding ability which has been confirmed in Fig. 4A. In general, the appropriate particle size and zeta potential of catiomer/pDNA complexes can facilitate the effective internalization into desired targeted cells.

Bio-responsive properties of the SL-ImPEG-SS-PLL/pDNA complexes

Stimulus-responsive polymeric nano-carriers have attracted increasing interest for both gene and drug delivery applications in recent years because they can greatly enhance the

intracellular release of the payload and usually exhibit lower cytotoxicity.[53–55] In this study, reversible-PEGylated polylysine (mPEG-SS-PLL$_{52}$) was developed for *in vivo* circulation as well as the selective detachment of PEG for facilitating the cellular internalization. While introducing Schiff-base linked imidazole residues into mPEG-SS-PLL$_{52}$, these were expected to further optimize the transfection efficiency of polylysine *via* increasing endosomal escape ability as well as DNA unpacking and release.

To confirm the proof of concept, size-alterations in the presence or absence of tumor-relevant GSH concentrations (*i.e.* 10 mM) were monitored by DLS and pH regulated DNA unpacking and release was investigated by agarose gel retardation assay. As shown in Fig. 6A, the exposure of SL-I$_{15}$mPEG-SS-PLL/pDNA complexes for 24 h to PBS, pH 7.4 in the absence of GSH did not significantly alter the particle size distribution implying substantial stability of these polyplexes during circulation. The inclusion of 10 mM GSH, however, rapidly increased the mean particle size, suggesting the formation of large aggregates (>680 nm) within 4 hours, which was due to the aggregation of cationic segments *via* ionic interactions after PEG detachment. Overall, these data suggest the feasibility of SL-ImPEG-SS-PLL for *in vivo* gene delivery as well as controllable PEG-shedding for the facilitation of cellular uptake. The results in Fig. 6B efficiently demonstrate the acidic pH condition regulated DNA unpacking and release. For example, pDNA migration at pH 7.4 was completely inhibited for SL-I$_{15}$mPEG-SS-PLL/pDNA complexes at weight ratios ≥0.15. However, incubation for 30 min at pH 5.0 results in visible pDNA migration using the same complexes at catiomer/pDNA ratios ≤1, which can be attributed to the decreased DNA binding ability with the hydrolysis of Schiff-base linkages in the weakly acidic endosomal compartment. This explanation is supported by the previous electrophoretic mobility data shown in Fig. 4A. In conclusion, these data underline the important role of Schiff-base linkages in regulating DNA unpacking and release.

Combined, these results imply that the synergistic effects of redox-induced PEG-shedding for the facilitation of cellular uptake, imidazole mediated proton sponge effect for the facilitation of genetic payload release into the cytoplasm as well as Schiff-base linkage regulated DNA unpacking and release, ultimately, may translate into high performance gene transfection efficiency (Scheme 1).

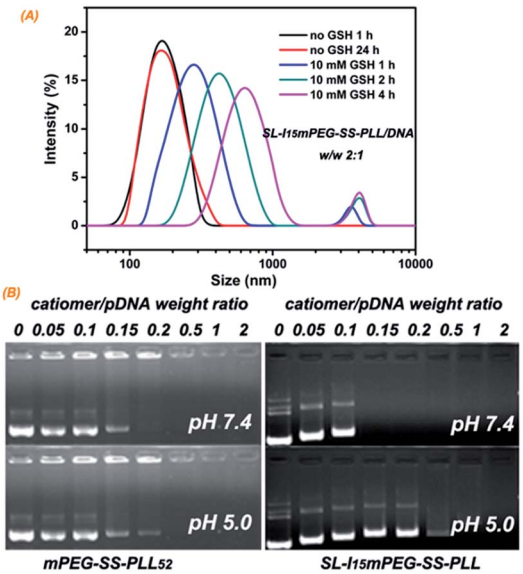

Fig. 6 Time-dependent changes in the size distribution of SL-I$_{15}$mPEG-SS-PLL/pDNA complexes as determined by DLS in the presence and absence of 10 mM GSH (A); stimulus-induced pDNA unpacking and release from the SL-I$_{15}$mPEG-SS-PLL/pDNA and mPEG-SS-PLL$_{52}$/pDNA complexes (B). Association complexes were incubated for 30 min in PBS, pH 7.4 or PBS, pH 5.0 before electrophoresis using a 1% agarose gel.

In vitro transfection studies of SL-ImPEG-SS-PLL/pDNA complexes

In vitro transfection experiments were performed on 293T and MCF-7 cells using EGFP and pGL-3 as reporter genes, and bPEI-25k at its optimal weight ratio 1.3 : 1 as the control. The catiomer/pEGFP weight ratio in the range of 1 : 1 to 4 : 1 was used for flow cytometry assay, which is higher than that used for complete DNA retardation. The weight ratios ranging from 0.5 : 1 to 4 : 1 were used for luciferase assay.

As shown in Fig. 7A and B, the calculated transfection efficiencies of mPEG-SS-PLL$_{52}$-, SL-ImPEG-SS-PLL- and PEI-based polyplexes exhibit cell-type dependence and a higher transfection activity is observed in the 293T cell line. For example, the calculated transfection efficiencies of viable cells in 293T cells are between 43% and 50%, for the mPEG-SS-PLL$_{52}$-based polyplexes. In contrast, those of viable cells in MCF-7 are in the range of 27–30% for the same polyplexes. Furthermore, the gene expression increases with increasing catiomer/pDNA weight ratio and gradually approaches saturation. The optimum weight ratios for mPEG-SS-PLL$_{52}$ and SL-ImPEG-SS-PLL-based catiomers are in the range of 2 to 3. Between the two kinds of carriers, SL-ImPEG-SS-PLL exhibits a better transfection activity and its transfection efficiency increases with increasing imidazole residues bound per mPEG-SS-PLL$_{52}$ molecule. The

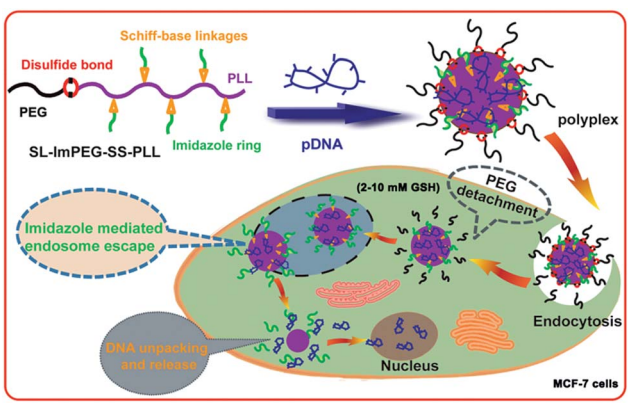

Scheme 1 Schematic illustration of SL-ImPEG-SS-PLL polyplex formation, subsequent intracellular PEG detachment, imidazole mediated endosomal escape, and Schiff-base regulated DNA unpacking and release.

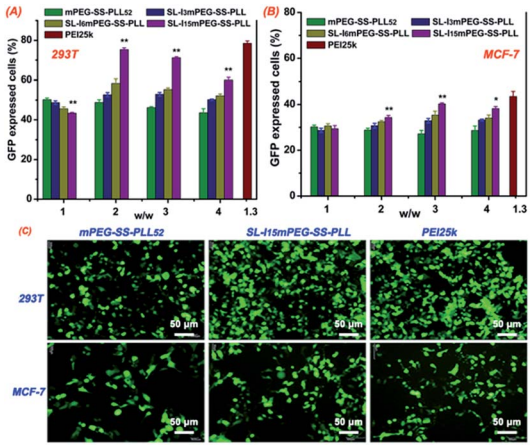

Fig. 7 Transfection efficiency of SL-ImPEG-SS-PLL-based polyplexes. 293T and MCF-7 cells are incubated for 4 h with these polyplexes fabricated at w/w ranging from 1 : 1 to 4 : 1; PEI polyplexes are used as control. Viable pEGFP-expressing cells are quantified after transfection for 44 h using flow cytometry and normalized to viable control cells (A and B). pEGFP-positive cells are identified 44 h after transfection by fluorescence microscopy (C) (*p < 0.05 and **p < 0.01, SL_{15}-ImPEG-SS-PLL polyplex *vs.* mPEG-SS-PLL_{52} polyplex).

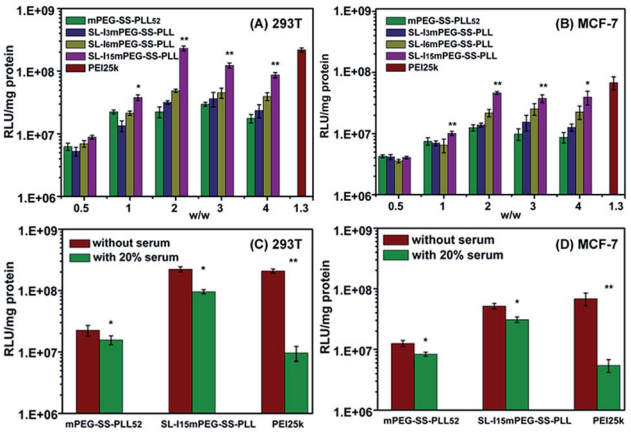

Fig. 8 Transfection efficiency of SL-ImPEG-SS-PLL-based polyplexes. 293T and MCF-7 cells are incubated for 4 h with these polyplexes fabricated at w/w ratios ranging from 0.5 : 1 to 4 : 1; PEI polyplexes are used as control. The luciferase activities of these polyplexes were identified 44 h after transfection by luciferase assay and normalized to viable control cells (A and B) (*p < 0.05, **p < 0.01, SL_{15}-ImPEG-SS-PLL polyplex *vs.* mPEG-SS-PLL_{52} polyplex). Data are shown as mean ± SD (n = 5). The effects of serum on luciferase transfection of SL-I_{15}mPEG-SS-PLL polyplexes are also assessed in the absence and presence of 20% serum (C and D) (*p < 0.05 and **p < 0.01, luciferase transfection with 20% serum *vs.* luciferase transfection without serum).

maximum transfection efficiency was achieved when 15 imidazole residues were incorporated into the side chains of mPEG-SS-PLL_{52}. At the weight ratio of 2, SL-I_{15}mPEG-SS-PLL has comparable transfection efficiency to bPEI-25k (78%), reaching up to 75%, which is 1.5-fold higher than that of mPEG-SS-PLL_{52} (50%). A similar tendency of EGFP-expression profiles of these polyplexes is observed from the fluorescence microscopy images (Fig. 7C). These data indicate the key role of Schiff-base linked imidazole residues in gene transfection. Following successful cellular internalization, the imidazole mediated endosomal escape as well as Schiff-base linkage regulated DNA unpacking and release, synergistically, result in the high performance gene delivery.

The luciferase activities of mPEG-SS-PLL_{52}-, SL-ImPEG-SS-PLL- and PEI-based polyplexes also experience cell type, weight ratio and carrier type dependencies (Fig. 8A and B). However, it is worth noting that the highest efficiency obtained for SL-I_{15}mPEG-SS-PLL polyplexes is 2.32×10^8 RLU mg^{-1} protein, approaching the same order of transgenetic efficacy as the bPEI-25k (2.18×10^8 RLU mg^{-1} protein) in the 293T cells, which is 7.7-fold higher than that of mPEG-SS-PLL_{52} polyplexes (2.98×10^7 RLU mg^{-1} protein). These results further indicate the important role of Schiff-base linked imidazole residues in optimizing gene transfection efficiency.

To achieve high stability of gene vectors in serum is a major goal in the design of the reversible PEGylation, which is essential for *in vivo* circulation.[56–58] In this study, the effects of serum on the transfection efficiency of the mPEG-SS-PLL_{52}-, SL-I_{15}mPEG-SS-PLL- and PEI-based polyplexes were assessed in the absence and presence of 20% serum. As shown in Fig. 8C and D, with 20% serum treatment, the transfection efficiency of PEI25k polyplexes undergoes about 22-fold and 13-fold lower luciferase expression in 293T and MCF-7 cells, respectively. Reduction in the transfection efficiency of PEI25k polyplexes is likely attributed to its instability in serum for their high surface charges. However, owing to the PEG-shielding effect, the transfection efficiencies of mPEG-SS-PLL_{52} and SL-I_{15}mPEG-SS-PLL polyplexes are slightly affected by serum. For example, they undergo only about 1.4-fold and 2.1-fold lower luciferase expression in 293T cells, respectively. These data suggest that SL-I_{15}mPEG-SS-PLL has great potential for *in vivo* gene delivery.

Cellular uptake and intracellular trafficking of catiomer/pDNA polyplexes

To explain the reason why reversible PEGylation and Schiff-base linked imidazole modification can efficiently increase the gene transfection efficiency of a PLL-based gene delivery system, we compared the cellular uptake efficiencies and intracellular trafficking behaviour of the mPEG-PLL_{52}/DNA, mPEG-SS-PLL_{52}/DNA and SL-I_{15}mPEG-SS-PLL/DNA polyplexes by confocal laser scanning microscopy (CLSM). As shown in Fig. 9, Cy3-labeled pEGFP signals (red fluorescent dots) are detected in almost all cells after 4 h treatment. However, the Cy3-labeled pEGFP signals delivered by mPEG-SS-PLL_{52}/DNA polyplexes in MCF-7 cells are stronger than those of mPEG-PLL_{52}/DNA polyplexes, implying the efficient cellular internalization. These observations clearly indicate that PEG detachment can significantly improve the cellular uptake efficiencies of the mPEG-PLL_{52}/DNA polyplexes. More importantly, stronger Cy3-labeled pEGFP signals are observed inside the nuclei of MCF-7 cells for SL-I_{15}mPEG-SS-PLL/DNA polyplexes, suggesting that imidazole mediated endosomal escape as well as Schiff-base linkage regulated DNA unpacking and release synergistically results in the efficient nucleus transport of pDNA. Combined, the efficient

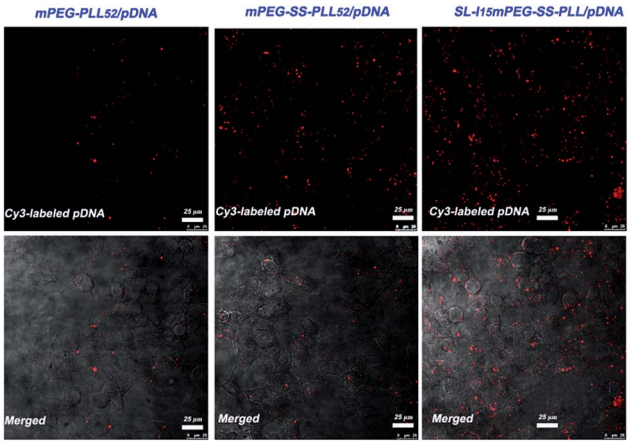

Fig. 9 Confocal microscopic images of cellular uptake and intracellular trafficking of mPEG-PLL_{52}/pDNA, mPEG-SS-PLL_{52}/pDNA and SL-I_{15}mPEG-SS-PLL/pDNA complexes. MCF-7 cells are incubated for 4 h with these complexes fabricated at each optimum weight ratios before CLSM observations.

cellular internalization, endosomal escape as well as nucleus transport of pDNA can explain why reversible PEGylation and Schiff-base linked imidazole modification can efficiently increase the gene transfection efficiency of a PLL-based gene delivery system.

In vivo gene expression in tumor-bearing mice

To explore the feasibility of SL-I_{15}mPEG-SS-PLL/DNA polyplexes for *in vivo* application, here, we investigated the transfection of pEGFP in various organs and xenografts in mice. Seven days after intravenous administration of SL-I_{15}mPEG-SS-PLL/DNA polyplexes, mice were sacrificed and the GFP expression in various sections was analyzed by CLSM. As shown in Fig. 10, GFP expression is found in the liver, spleen, kidneys, lungs, and tumor of the mice. The fluorescence intensities in the liver and spleen are found to be much stronger than those in other organs. This behaviour is possibly associated with the reticuloendothelial system (RES) or mononuclear phagocyte system (MPS). A relatively high fluorescence intensity is also observed in tumor, suggesting that SL-I_{15}mPEG-SS-PLL is a promising gene vector for bio-application. A sufficient long circulation of SL-I_{15}mPEG-SS-PLL in the bloodstream was found during effective gene expression *in vivo*. The vector coated with mPEG shells successfully circulated in vasculature rather than being aggregated and precipitated with negatively charged serum proteins in vasculature.

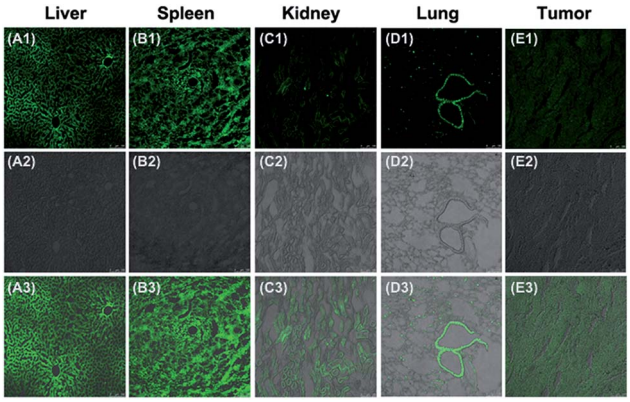

Fig. 10 Confocal microscopy images of transfected sections of the (A) liver, (B) spleen, (C) kidney, (D) lung, and (E) tumor after intravenous injection of the SL-I_{15}mPEG-SS-PLL/pEGFP polyplex (w/w, 2 : 1, dose: 100 μg pEGFP per mice) 7 days. Row 1 and Row 2 show the images of the fluorescent and bright fields, respectively. The images of Row 3 are merged images of Row 1 and Row 2. Images are captured at 20×.

Conclusions

In this study, we have designed and developed an intracellular microenvironment responsive gene delivery vector, namely Schiff-base linked imidazole modified polylysine with a reversible-PEGylation (SL-ImPEG-SS-PLL) cationer according to the specific gene delivery requirements. The reversible PEGylation allows the protection of the cationer/pDNA polyplexes as well as selective PEG detachment, which is essential to cell internalization. Following efficient cellular internalization, the imidazole mediated endosomal escape and Schiff-base linkage regulated DNA unpacking and release, synergistically, enhanced the biological efficacy of the PLL-based gene delivery system. Furthermore, this new delivery system has good biocompatibility but high *in vivo* transfection efficiency. Such a system should have promising applications in the future gene therapy.

Materials and methods

Chemicals and reagents

Poly(ethylene glycol) monomethyl ether (mPEG, M_w = 2000 g mol^{-1}) was purchased from Yare Biotech (China). ε-Benzyloxycarbonyl-L-lysine was purchased from GL Biochem., Ltd. Triphosgene (99%) was purchased from Aladdin (China) and used as received. 4-Imidazolecarboxaldehyde (98%) was purchased from Aldrich-Sigma Chemical (USA). Hydrogen bromide 33% (w/w) solution in glacial acetic acid was purchased from ACROS Organics (USA). *N*,*N*-Dimethyl formamide (DMF) was purchased from Sigma Aldrich (China) and used as received. Tetrahydrofuran (THF) and dichloromethane (DCM) were dried by refluxing over CaH_2, distilled, or vacuum-distilled before use. Dialysis bags (Spectra/Por 7) were purchased from Spectrum Laboratories (China). Dulbecco's modified Eagle's medium (DMEM), fetal bovine serum (FBS), penicillin–streptomycin, Dulbecco's phosphate buffered saline (DPBS), 3-(4,5-dimethyl-thiazol-2-yl)-2,5-diphenyltetrazolium bromide (MTT) and trypsin–EDTA were purchased from Gibco Invitrogen (USA). The reporter plasmids, pEGFP-C1 and pGL-3, were purchased from Invitrogen (USA) and stored at −20 °C until transfection experiments. Branched poly(ethylenimine) (bPEI-25k, M_w = 25 000 g mol^{-1}) was obtained from Aldrich-Sigma Chemical (USA). A BCA protein assay kit was purchased from the Beyotime Institute of Biotechnology (Beijing, China). A Label IT Tracker intracellular nucleic acid localization kit Cy3 was purchased from Mirus Bio (USA).

Synthesis of Schiff-base linked imidazole modified polylysine with reversible-PEGylation (SL-ImPEG-SS-PLL)

The Schiff-base linked imidazole modified polylysine with a reversible-PEGylation catiomer (SL-ImPEG-SS-PLL) was synthesized as follows: the mPEG-SS-PLL_{52} copolymer was prepared by the ring-opening polymerization of zLL-NCA using mPEG-SS-NH_2 as the initiator, followed by deprotection of the Z groups. The primary amines of PLL were then partially replaced by imidazole rings in water with 4-imidazolecarboxaldehyde.

mPEG-SS-PLL_{52} was prepared following a protocol published previously.[37] Briefly, the mPEG-SS-NH_2 and zLL-NCA intermediates mPEG-SS-PzLL were synthesized by the ring-opening polymerization of zLL-NCA, initiated by mPEG-SS-NH_2 at a moral ratio of 60 : 1, and the desired product was obtained by deprotection of the Z groups. As a control material, mPEG-PLL_{52} was also synthesized by the ring-opening polymerization of zLL-NCA initiated by mPEG-NH_2 in DMF under the same conditions according to mPEG-SS-PLL_{52}. The structure of mPEG-SS-PLL_{52} was confirmed by Proton nuclear magnetic resonance (^{1}H NMR) using an Advance500 MHz spectrometer (Bruker BioSpin, Switzerland). Samples were dissolved in D_2O and TMS was used as the standard.

In a typical experiment for SL-ImPEG-SS-PLL synthesis, mPEG-SS-PLL_{52} (0.5 g, 0.057 mmol) was dissolved in 20 mL deionized water, and an aqueous solution of 4-imidazolecarboxaldehyde (0.028 g, 0.296 mmol or 0.057 g, 0.593 mmol or 0.114 g, 1.186 mmol) was added dropwise over 1 h under vigorous stirring at RT. The reaction mixture was stirred for an additional 4 h before dialysis (M_w cutoff: 3500 Da) for 24 h against water. The purified SL-ImPEG-SS-PLL was collected after lyophilization. The average number of imidazole groups bound per mPEG-SS-PLL_{52} molecule was determined by ^{1}H NMR.

Cell culture and viability assay

Human embryonic kidney transformed 293 (293T) and human breast cancer cells (MCF-7) were obtained from the Cell Center of the Tumor Hospital at Fudan University and routinely maintained at 37 °C in a humidified 5% (v/v) CO_2 atmosphere using DMEM supplemented with 10% FBS and 0.1% (v/v) penicillin/streptomycin solution.

The cytotoxicity of the fabricated catiomer was determined on 293T and MCF-7 cells by the MTT assay.[59] Briefly, 293T and MCF-7 cells were seeded into a 96-well plate at a density of 5×10^3 cells per well. Following an overnight attachment period, cells were exposed to various catiomer concentrations (13.2 to 225 mg L^{-1}) prepared in cell culture medium. After 24 h, the medium was replaced with 200 μL of fresh DMEM containing 10% FBS, 20 μL of a MTT solution (5 mg mL^{-1}) in PBS at pH 7.4, and the plate incubated at 37 °C for an additional 4 h. 150 μL of DMSO was subsequently added to each well. After an additional 10 min incubation at 37 °C, optical density (OD) was measured at $\lambda = 492$ nm using a Multiscan MK3 plate reader (Thermo Fisher Scientific, Waltham, MA, USA). The relative cell viability in percent (%) was calculated according to: (OD sample/OD control) × 100%, where OD control was measured without the presence of the polymers. Each concentration was studied using six independent experiments.

Buffering capacity of SL-ImPEG-SS-PLL catiomers

The relative buffering capacities of SL-ImPEG-SS-PLL catiomers were measured by titration according to the method described by Tseng with PEI25k as control.[60] Polymers were dissolved in 200 mg L^{-1} of 50 mM NaCl solution. Initially, the pH value of the solution was adjusted to pH = 10 using 0.1 N NaOH. 0.1 N HCl aliquots were then added, and the pH value was measured after each addition using a microprocessor pH meter.

Assembly and characterization of SL-ImPEG-SS-PLL/pDNA complexes

DNA complex assembly. The SL-ImPEG-SS-PLL-based catiomer/pDNA complexes at various weight ratios ranging from 0.05 : 1 to 2 : 1 were prepared by adding appropriate volumes of mPEG-SS-PLL_{52} or SL-ImPEG-SS-PLL solutions (2 mg mL^{-1} in 150 mM NaCl solution) to 0.5 μg of pEGFP DNA (160 ng μL^{-1} in 40 mM Tris–HCl buffer solutions). The complexes were then vortexed gently for 3 s, and incubated at 37 °C for 30 min to allow complete formation.

Gel electrophoresis assay. The agarose gel retardation assay was performed to assess the ability of catiomers to condense pDNA into the electrostatically stabilized polyplexes. Routinely, catiomer/pDNA complex suspensions containing 0.5 μg of pDNA was loaded onto 1% (w/v) agarose gel containing ethidium bromide. Electrophoretic separation was carried out for 40 min at 120 V in Tris–acetate running buffer. DNA bands were visualized at $\lambda = 254$ nm using the Imago GelDoc system.

Particle size, zeta potential and morphology measurement of DNA complexes

To determine relevant physicochemical properties of polyplexes, particle size distribution and zeta potential of fabricated catiomer/pDNA complexes were respectively measured by using a dynamic laser light scattering (DLS) instrument and a Nano-ZS 90 Nanosizer (Malvern Instruments Ltd., Worcestershire, UK) according to the manufacturer's instructions. When required, the polyplex suspension was diluted with 150 mM NaCl (pH 7.4). To investigate the structure of the catiomer/pDNA complexes, SL-ImPEG-SS-PLL/pDNA polyplexes were prepared at a weight ratio of 2 : 1 and observed on a Hitachi H-7100 transmission electron microscope (TEM) using an acceleration voltage of 100 kV.

Complex stability under intracellular reductive or endosomal acidified conditions

The protocol used to assess the complex stability in response to GSH was adapted from the literature.[61] Typically, SL-I_{15}mPEG-SS-PLL/pDNA complexes were formed in 150 mM NaCl at a weight ratio of 2 : 1, and an adequate amount of GSH was added to establish a 10 mM GSH solution mimicking intracellular or tumor microenvironment redox conditions. Time-dependent changes in the particle size distribution of this suspension was monitored by dynamic laser light scattering (DLS) for up to 4 h.

To evaluate the complex stability under the endosomal acidified conditions, mPEG-SS-PLL$_{52}$/pDNA and SL-I$_{15}$mPEG-SS-PLL/pDNA complexes was formed in 150 mM NaCl at desired weight ratios, then an adequate volume of HCl was added to adjust the solution pH to 5.0. Following 30 min incubation, aliquots of the polyplex suspension conditions were removed and subjected to gel electrophoresis as described above.

In vitro transfection efficiency

The biological activity of fabricated gene delivery vectors was assessed *in vitro* using EGFP and pGL-3 as reporter genes. PEI25k at its optimal ratio (w/w = 1.3 : 1) served as control. Transfection experiments were performed with 293T and MCF-7 cells in 24-well plates at a density of 5×10^4 cells per well.

For the flow cytometry study, pEGFP-containing polyplexes with catiomer/pDNA weight ratios ranging from 1 : 1 to 4 : 1 were suspended in serum-free DMEM for each well (0.5 μg DNA per well). After 4 h incubation at 37 °C in a humidified atmosphere with 5% (v/v) CO_2, the transfection medium was replaced with fresh complete DMEM medium. At 44 h post-transfection, pEGFP-expressing cells were first visualized under a Nikon Ti–S inverted microscope equipped with a fluorescence attachment. For flow cytometry assessment, cells were washed with PBS, pH 7.4, trypsinized, and collected in sterile tubes after a 5 min centrifugation at 1000 rpm. The supernatant was discarded and cells were washed twice with PBS, pH 7.4 containing 2% (v/v) FBS, and 2 mM EDTA, respectively. Cells were fixed in the dark at 4 °C for 5 min using a 2% (w/v) paraformaldehyde solution prepared in PBS, pH 7.4. Quantitative analysis of viable EGFP-expressing cells was performed by flow cytometry (FACScan, Becton & Dickinson). The instrument was calibrated with non-transfected cells (negative control) to identify viable cells, and the percent of EGFP-positive cells was determined by a fluorescence scan performed with $\sim 1 \times 10^4$ cells using a FL1-H channel.

For luciferase assay, pGL-3-containing polyplexes were separately transferred to the 293T and MCF-7 cells in terms of the aforementioned method. After 4 h incubation at 37 °C in a humidified atmosphere with 5% (v/v) CO_2, the transfection medium was replaced with fresh complete DMEM medium. Forty-four hours later, cells were washed with 0.25 mL of cold PBS, pH 7.4, then the cells were lysed using 200 μL of reporter lysis buffer (Promega, USA). The luciferase activity was measured with a chemiluminometer (GloMax-Multi, Promega, USA) according to the manufacturer's protocol. Luciferase activity was normalized to the amount of total protein in the sample, which was determined using a BCA protein assay kit (Pierce). The biological efficiency of the SL-ImPEG-SS-PLL catiomer in 293T and MCF-7 cells in the presence or absence of 20% FBS was also evaluated according to the same procedures described above.

Cellular uptake and intracellular trafficking of catiomer/pDNA polyplexes

Cellular uptake and intracellular trafficking of mPEG-SS-PLL$_{52}$ and SL-I$_{15}$mPEG-SS-PLL polyplexes were evaluated using confocal laser scanning microscopy (CLSM). MCF-7 cells were seeded at a density of 2×10^5 cells per well in a 6-well plate containing a coverslip in each well. Five μg pEGFP was intercalated with 5 μL of 10 mM Cy3 for 60 min at 37 °C before the addition of a catiomer.[62] Subsequently, labeled pEGFP was purified by precipitating twice in cold ethanol 100%, rinsing in ethanol 70%, and then resuspended in 10 μL of sterile water. The Cy3-labeled pEGFP-containing polyplexes (w/w = 2 : 1, 1 μg DNA per well) were prepared and added to each well. Following 4 h incubation at 37 °C, the cells were rinsed twice with PBS, pH 7.4, to remove polyplexes that were not taken up by cells. The intracellular localization of DNA complexes was observed by the excitation of Cy3 at 570 nm and detection of emission at 650 nm using a confocal laser scanning microscope (CLSM, Leica TCS SP5).

Animal and subcutaneous tumor implantation

Healthy female BALB/c nude mice (16–20 g, 4–5 weeks old) were purchased from the BK Lab Animal Ltd/Animal Biosafety Level 3 Laboratory (ABSL-3 lab) (Shanghai, China), and housed at Tongji University Experimental Animal Center (ABSL-3 lab) under specific pathogen-free conditions according to Institution Animal Care and Use guidelines, using a laminar airflow rack. Animals possessed continuous access to sterilized food pellets and distilled water, and a 12 h light/dark cycle, temperature 23 °C, with a relative humidity of 50–60%. All experimental procedures were conducted according to the Institutional Animal Care and Use guidelines. For the subcutatenous MCF-7 (female nude mice) xenograft model, about 1×10^7 MCF-7 cells in a volume of 100 μL of PBS were inoculated subcutaneously into the left flank region of BALB/c nude mice.

In vivo EGFP reporter gene expression

When the subcutaneous MCF-7 tumor grew to a size range, approximately between 50 mm and 80 mm in diameter, 150 μL of SL-I$_{15}$mPEG-SS-PLL/pDNA complexes (w/w = 2/1, 100 μg DNA per mice) was injected into the tail vein of the nude mice bearing a subcutaneous MCF-7 xenograft tumor. Upon 7 day post-injection, mice were sacrificed and the tumors, livers, spleens, kidneys and lungs were removed, fixed with 4% paraformaldehyde, dehydrated with 10%, 20% and 30% sucrose solutions for 24 h sequentially, and then embedded in OCT embedding fluid (Jung, Leica) and thinly sectioned (~10 μm histology slice) on a cryostat microtome (Cryocut 3000, Leica). The obtained sections were visualized and recorded using a Leica TCS SP5 II fluorescence microscope to evaluate the EGFP expression in various organs.

Statistical analysis

Data are presented as mean ± standard deviations (±S.D.) of at least five independent samples and each measurement was performed in triplicate. Statistical analysis was determined by analysis of variance tests (ANOVA) using Microsoft Excel 2007. Data sets were compared using two-tailed software *t*-tests. And a p value <0.05 was considered to be statistically significant.

Acknowledgements

This work was financially supported by the 973 program (no. 2013CB967500, 2011CB606206), the National Science Foundation of China (no. 21104059, 51173136 and 51133004), the Shanghai Rising-Star Program (12QA1403400) and the "Chen Guang" project funded by the Shanghai Municipal Education Commission, the Shanghai Education Development Foundation and the China postdoctoral fund (2014M552359). The authors are grateful to the Scientific and Technological Research Program of the Chongqing Municipal Education Commission (grant no. KJ130820).

Notes and references

1 P. S. Ghosh, C.-K. Kim, G. Han, N. S. Forbes and V. M. Rotello, *ACS Nano*, 2008, **2**, 2213–2218.
2 C. Ornelas-Megiatto, P. R. Wich and J. M. Frèchet, *J. Am. Chem. Soc.*, 2012, **134**, 1902–1905.
3 B. Y. Shi, H. Zhang, S. Dai, X. Du, J. X. Bi and S. Z. Qiao, *Small*, 2014, **10**, 871–877.
4 Y. M. Li, J. H. Yang, L. Sun, W. Wang and W. G. Liu, *J. Mater. Chem. B*, 2014, **2**, 3868–3878.
5 Y. Nie, D. Schaffert, W. Rödl, M. Ogris, E. Wagner and M. Günther, *J. Controlled Release*, 2011, **152**, 127–134.
6 H. Wei, L. R. Volpatti, D. L. Sellers, D. O. Maris, I. W. Andrews, A. S. Hemphill, L. W. Chan, D. S. H. Chu, P. J. Horner and S. H. Pun, *Angew. Chem., Int. Ed.*, 2013, **52**, 5377–5381.
7 Y. R. Liu, Y. J. Kim, M. Ji, J. X. Fang, N. Siriwon, L. I. Zhang and P. Wang, *Mol. Ther. Methods Clin. Dev.*, 2014, **1**, 12.
8 Y. R. Liu, Y. Fang, Y. Zhou, E. Zandi, C. L. Lee, K.-I. Joo and P. Wang, *Small*, 2013, **9**, 421–429.
9 Z. Q. Yu, B. Yu, J. B. Kaye, C. H. Tang, S. Cheng, C. B. Dong and B. Shen, *Nano LIFE*, 2014, **4**, 1441016.
10 E. R. Figueroa, A. Y. Lin, J. X. Yan, L. Luo, A. E. Foster and R. A. Drezek, *Biomaterials*, 2014, **35**, 1725–1734.
11 X. J. Cai, H. Q. Dong, J. P. Ma, H. Y. Zhu, W. Wu, M. Chu, Y. Y. Li and D. L. Shi, *J. Mater. Chem. B*, 2013, **1**, 1712–1721.
12 H. Y. Tian, J. Chen and X. S. Chen, *Small*, 2013, **9**, 2034–2044.
13 K. Luo, C. X. Li, G. Wang, Y. Nie, B. He, Y. Wu and Z. W. Gu, *J. Controlled Release*, 2011, **155**, 77–87.
14 F. Y. Dai and W. G. Liu, *Biomaterials*, 2011, **32**, 628–638.
15 H. Y. Tian, Z. P. Guo, J. Chen, L. Lin, J. L. Xia, X. Dong and X. S. Chen, *Adv. Healthcare Mater.*, 2012, **1**, 337–341.
16 X. J. Cai, H. Y. Zhu, H. Q. Dong, Y. Y. Li, J. S. Su and D. L. Shi, *Adv. Healthcare Mater.*, **3**, 1818–1827.
17 Y. Y. He, Y. Nie, G. Cheng, L. Xie, Y. Q. Shen and Z. W. Gu, *Adv. Mater.*, 2013, **26**, 1534–1540.
18 Y. H. Wang, M. Zheng, F. H. Meng, J. Zhang, R. Peng and Z. Y. Zhong, *Biomacromolecules*, 2011, **12**, 1032–1040.
19 X. Zhang, M. O. Abdelghani, A. N. Zelkin, Y. J. Wang, Y. Haîkel, D. Mainard, J.-C. Voegel, F. Caruso and N. B. Jessel, *Biomaterials*, 2009, **31**, 1699–1706.
20 M. Sanjoh, S. Hiki, Y. Lee, M. Oba, K. Miyata, T. Ishii and K. Kataoka, *Macromol. Rapid Commun.*, 2010, **31**, 1181–1186.
21 M. M. Wang, H. M. Liu, L. Li and Y. Y. Cheng, *Nat. Commun.*, 2014, **5**, 3053–3060.
22 X. J. Wang, N. M. Shao, Q. Zhang and Y. Y. Cheng, *J. Mater. Chem. B*, 2014, **2**, 2546–2553.
23 H. M. Liu, H. Wang, W. J. Yang and Y. Y. Cheng, *J. Am. Chem. Soc.*, 2012, **134**, 17680–17687.
24 F. Y. Dai, P. Sun, Y. J. Liu and W. G. Liu, *Biomaterials*, 2010, **31**, 559–569.
25 S. R. Yu, J. X. Chen, R. J. Dong, Y. Su, B. Ji, Y. F. Zhou, X. Y. Zhu and D. Y. Yan, *Polym. Chem.*, 2012, **3**, 3324–3329.
26 J. Wu, D. Yamanouchi, B. Liu and C. C. Chu, *J. Mater. Chem.*, 2012, **22**, 18983–18991.
27 Y. T. Wen, Z. X. Zhang and J. Li, *Adv. Funct. Mater.*, 2014, **24**, 3874–3884.
28 Y. Y. Yue and C. Wu, *Biomater. Sci.*, 2013, **1**, 152–170.
29 X. J. Cai, C. Y. Dong, H. Q. Dong, G. M. Wang, G. M. Paulletti, X. J. Pan, H. Y. Wen, I. Mehl, Y. Y. Li and D. L. Shi, *Biomacromolecules*, 2012, **13**, 1024–1034.
30 D. W. Pack, A. S. Hoffman, S. Pun and P. S. Stayton, *Nat. Rev. Drug Discovery*, 2005, **4**, 581–593.
31 V. P. Torchilin, *Adv. Drug Delivery Rev.*, 2012, **64**, 302–315.
32 A. E. Aneed, *J. Controlled Release*, 2004, **94**, 1–14.
33 S. Y. Wong, J. M. Pelet and D. Putnam, *Prog. Polym. Sci.*, 2007, **32**, 799–837.
34 C. M. Ward, M. L. Read and L. W. Seymour, *Blood*, 2001, **97**, 2221–2229.
35 T. Merdan, J. Kopeček and T. Kissel, *Adv. Drug Delivery Rev.*, 2002, **54**, 715–758.
36 D. Z. Zhou, C. X. Li, Y. L. Hu, H. Zhou, J. T. Chen, Z. P. Zhang and T. Y. Guo, *J. Mater. Chem.*, 2012, **22**, 10743–10751.
37 X. J. Cai, H. Q. Dong, W. J. Xia, H. Y. Wen, X. Q. Li, J. H. Yu, Y. Y. Li and D. L. Shi, *J. Mater. Chem.*, 2011, **21**, 14639–14645.
38 B. Y. Shi, H. Zhang, J. X. Bi and S. Dai, *Colloids Surf., B*, 2014, **119**, 55–65.
39 B. Y. Shi, H. Zhang, Z. Y. Shen, J. X. Bi and S. Dai, *Polym. Chem.*, 2013, **4**, 840–850.
40 T. H. Kim, J. E. Ihm, Y. J. Choi, J. W. Nah and C. S. Cho, *J. Controlled Release*, 2003, **93**, 389–402.
41 B. Ghosn, A. Singh, M. Li, A. V. Vlassov, C. Burnett, N. Puri and K. Roy, *Oligonucleotides*, 2010, **20**, 163–172.
42 R. Chandra and R. Rustgi, *Prog. Polym. Sci.*, 1998, **23**, 1273–1335.
43 J. Liang, G. Steinberg, N. Livnah, M. Sheves and T. G. Ebrey, *Biophys. J.*, 1994, **67**, 848–854.
44 Y. Li and Z. Y. Yang, *Inorg. Chim. Acta*, 2009, **362**, 4823–4831.
45 Y. Xin and J. Y. Yuan, *Polym. Chem.*, 2012, **3**, 3045–3055.
46 S. Y. Duan, W. E. Yuan, F. Wu and T. Jin, *Angew. Chem., Int. Ed.*, 2012, **51**, 1–5.
47 D. Fischer, T. Bieber, Y. X. Li, H. P. Elsässer and T. Kissel, *Pharm. Res.*, 1999, **16**, 1273–1279.
48 R. Goyal, R. Bansal, S. Tyagi, Y. Shukla, P. Kumar and K. C. Gupta, *Mol. BioSyst.*, 2011, **7**, 2055–2065.
49 K. Osada and K. Kataoka, *Adv. Polym. Sci.*, 2006, **202**, 113–153.
50 S. E. A. Gratton, P. A. Ropp, P. D. Pohlhaus, J. C. Luft, V. J. Madden, M. E. Napier and J. M. Desimone, *Proc. Natl. Acad. Sci. U. S. A.*, 2008, **105**, 11613–11618.

51 R. L. Sheng, T. Luo, Y. D. Zhu, H. Li, J. J. Sun, S. D. Chen, W. Y. Sun and A. Cao, *Biomaterials*, 2011, **32**, 3507–3519.
52 Y. M. Liu and T. M. Reineke, *J. Am. Chem. Soc.*, 2005, **127**, 3004–3015.
53 T.-i. Kim and S. W. Kim, *React. Funct. Polym.*, 2011, **71**, 344–349.
54 Z. Q. Yu, J. J. Yan, Y. Z. You and Q. H. Zhou, *Int. J. Nanomed.*, 2012, **7**, 5819–5832.
55 H. H. Xiao, R. G. Qi, S. Liu, X. L. Hu, T. C. Duan, Y. H. Zheng, Y. B. Huang and X. B. Jing, *Biomaterials*, 2011, **32**, 7732–7739.
56 K. Miyata, M. Oba, M. R. Kano, S. Fukushima, Y. Vachutinsky, M. Han, H. Koyama, K. Miyazono, N. Nishiyama and K. Kataoka, *Pharm. Res.*, 2008, **25**, 2924–2936.
57 S. Fukushima, K. Miyata, N. Nishiyama, N. Kanayama, Y. Yamasaki and K. Kataoka, *J. Am. Chem. Soc.*, 2005, **127**, 2810–2811.
58 R. G. Qi, S. Liu, J. Chen, H. H. Xiao, L. S. Yan, Y. B. Huang and X. B. Jing, *J. Controlled Release*, 2012, **159**, 251–260.
59 B. R. Schroeder, M. I. Ghare, C. Bhattacharya, R. Paul, Z. Q. Yu, P. A. Zaleski, T. C. Bozeman, M. J. Rishel and S. M. Hecht, *J. Am. Chem. Soc.*, 2014, **136**, 13641–13656.
60 W. C. Tseng, C. H. Tang and T. Y. Fang, *J. Gene Med.*, 2004, **6**, 895–905.
61 H. L. Sun, B. N. Guo, X. Q. Li, R. Cheng, F. H. Meng, H. Y. Liu and Z. Y. Zhong, *Biomacromolecules*, 2010, **11**, 848–854.
62 J. Dai, S. Y. Zou, Y. Y. Pei, D. Cheng, H. Ai and X. T. Shuai, *Biomaterials*, 2011, **32**, 1694–1705.